2018-08

Target Motion Estimation Ambiguities for Monostatic Synthetic Aperture Radar

Garren, David Alan

IEEE

Correspondence

Target Motion Estimation Ambiguities for Monostatic Synthetic Aperture Radar

A recent analysis demonstrates that ambiguities exist in attempting to estimate target motion for general bistatic synthetic aperture radar collections. However, monostatic geometries appear to be problematic, since two coordinate angles become indeterminate. The current investigation resolves these issues and provides new insights into the nature of these ambiguities.

I. INTRODUCTION

Synthetic aperture radar (SAR) image formation is used to acquire the intelligence regarding stationary scenes in all weather conditions. However, objects with motion are mismatched with the SAR processing and, thus, typically yield smeared signatures. A number of investigations [1]–[9], [10] have attempted to use such induced imagery artifacts together with various assumptions in order to determine motion parameters. One possible analysis method (e.g., [5]) is to assume that the target motion follows a low-order parametric form exactly, as with constant velocity or acceleration. The resulting equations can be inverted uniquely to yield values for the target motion parameters. However, a number of investigators [11]–[15] present specific scenario examples wherein any attempt to estimate the target location and other motion parameters corresponding to an induced smeared target artifact yields ambiguities. Additional constraints must be applied in order to break these ambiguities, as with the case of prior knowledge that a given target is traveling on a particular road or via the use of additional receiver phase centers [16], [17].

Garren [18] presents the results of recent investigation which considers these ambiguities for cases of general bistatic geometries with arbitrary motions for the radar transmitter and receiver. This analysis provides the specific equations for generating any number of alternative fictitious target trajectories and speed profiles on the surface of a ground-plane which yield an identical set of bistatic range measurements of any given surface target with arbitrary motion. Thus, it is not possible to apply a single set of range measurement data to obtain an accurate estimate of the target motion. These results apply even if range-rate or Doppler measurements are collected as well. Garren [19] extends the earlier ambiguity analysis [18] so as to apply for "air targets" which have freedom to move in three dimensions (3D).

Manuscript received July 14, 2017; revised December 29, 2017; released for publication December 29, 2017. Date of publication February 2, 2018; date of current version August 7, 2018.

DOI. No. 10.1109/TAES.2018.2801618

Refereeing of this contribution was handled by S. Watts.

The analyses of the prior publications [18], [19] appear to be problematic for the degenerate case of monostatic geometries. Specifically, two coordinate transformation angles are indeterminate if the receiver location is exactly equal to that of the transmitter. Garren [20] applies a workaround via the inclusion of a small but nonzero separation between the radar transmitter and receiver for each waveform. However, such a kluge is unsatisfactory from a theoretical perspective. The current analysis develops the required modifications of the equations for generating alternate fictitious target trajectories and speed profiles for the monostatic case. Furthermore, the resulting simplified equations provide enhanced insights into the nature of these target motion ambiguities.

Section II summarizes the background of the ambiguity equations for general bistatic geometries. Section III develops simplified ambiguity equations for monostatic collections. Section IV generates multiple alternate fictitious target trajectories and speed profiles for a selected example. The conclusions are provided in the final section.

II. BISTATIC COLLECTIONS

A summary of the apparent difficulties in the general bistatic ambiguity equations for the degenerate case of monostatic geometries is provided below. For brevity, any repetition from previous works [18]–[20] is minimized to include only the equations required to enable an understanding of the current monostatic ambiguity analysis.

A. True Target Trajectory

The bistatic ambiguity analysis [18] permits the transmitter and receiver to move with arbitrary trajectories and speed profiles in time and to be known with arbitrary precision. In addition, the unknown target motion is arbitrary except that it must lie on the surface of the ground-plane. The transmitter emanates N radar waveforms during the SAR collection interval. Let $\tau_{t,n}$ be the transmission time of the nth waveform, and denote $\tau_{r,n}$ to be the time of waveform reception after scattering of the target. Furthermore, the time duration between successive waveforms can vary arbitrarily.

Select local Cartesian coordinates $\{x, y, z\}$ wherein the $z = 0$ plane is tangent to the earth's surface. Denote the target location at the waveform scattering time $\tau_{s,n}$ via $\mathbf{x}_{s,n} = \{x_{s,n}, y_{s,n}, 0\}$. Garren [18] forms the 3-D ambiguity ellipsoid by revolving a two-dimensional (2-D) ellipse around the axis connecting the transmitter and receiver, which correspond to the two foci. Denote $\mathbf{x}_{t,n} = \{x_{t,n}, y_{t,n}, z_{t,n}\}$ to be the transmitter phase center location at the time $\tau_{t,n}$, and let $\mathbf{x}_{r,n} = \{x_{r,n}, y_{r,n}, z_{r,n}\}$ be the receiver phase center location at the time $\tau_{r,n}$. A given bistatic radar range measurement is denoted by R_n. Furthermore, the bistatic range measurement error δR_n can be arbitrarily small, since the radar bandwidth is permitted to be arbitrarily wide.

B. Alternate Target Construction

Garren [18] presents a prescription for computing any number of alternate fictitious target trajectories and speed profiles which give the same set of bistatic range measurements as that of the true target motion. The target motion parameters of a given alternate target trajectory are not restricted to be approximately that of the true target. The only constraint is that the fictitious target location lies in the overlap of the transmission and reception beampatterns for each waveform.

The round-trip waveform propagation fast-time $\Delta\tau$ and the bistatic range R are related via

$$\Delta\tau \equiv \tau_r - \tau_t = \frac{2R}{c}. \tag{1}$$

The waveform index n is suppressed to make the notion less cumbersome. The center of the 3-D ellipsoid is $\mathbf{x}_0 \equiv \{\mathbf{x}_r + \mathbf{x}_t\}/2$ in terms of the transmission and reception phase center locations, $\mathbf{x}_t$ and $\mathbf{x}_r$, respectively. Also, this ellipsoid center has the form $\{x, y, z\} = \{X_0, Y_0, Z_0\}$ in terms of the selected ground-plane coordinates.

Rotation angles which define the orientation of the 3-D ellipsoid relative to the ground-plane require the definition of the vector between the transmitter and receiver locations:

$$\mathbf{w} \equiv \mathbf{x}_r - \mathbf{x}_t. \tag{2}$$

Denote the Cartesian components of $\mathbf{w}$ along the ground-plane unit vectors $\{\hat{\mathbf{x}}, \hat{\mathbf{y}}, \hat{\mathbf{z}}\}$ via $\{w_x, w_y, w_z\}$. Then, Garren [18] provides the definitions of the elevation Φ and azimuthal Θ angles of the 3-D ellipsoid relative to the ground-plane coordinates via

$$-\frac{\pi}{2} \le \Phi \equiv \arctan\left(\frac{w_z}{\sqrt{w_x^2 + w_y^2}}\right) \le \frac{\pi}{2} \tag{3}$$

$$-\pi < \Theta \equiv \arctan\left(\frac{w_y}{w_x}\right) \le \pi. \tag{4}$$

Here, the signs of the values of w_x and w_y determine the quadrant of Θ. Specifically, a positive value of w_y implies that Θ lies between zero and π. Likewise, a negative w_y restricts Θ to be in the interval between $-\pi$ and zero.

The vector $\mathbf{w}$ of (2) is zero for monostatic SAR, so that the definitions of Φ and Θ in (3) and (4) are indeterminate. A resolution of this issue is developed in Section III.

Garren [18] generates the 3-D ambiguity ellipsoid via

$$\sum_{0\le\alpha+\beta+\gamma\le 2} p_{\alpha\beta\gamma}\; x^\alpha y^\beta z^\gamma = 0. \tag{5}$$

In this equation, the $p_{\alpha\beta\gamma}$ functions are defined by

$$p_{200} \equiv \rho, \qquad p_{020} \equiv \omega, \qquad p_{002} \equiv \gamma \tag{6}$$

$$p_{110} \equiv \{\psi - \eta\}\sin(2\Theta) \tag{7}$$

$$p_{011} \equiv \{\xi - \eta\}\sin(\Theta)\sin(2\Phi) \tag{8}$$

$$p_{101} \equiv \{\xi - \eta\}\cos(\Theta)\sin(2\Phi) \tag{9}$$

$$p_{100} \equiv -2X_0\,\rho - Y_0\{\psi - \eta\}\sin(2\Theta) - Z_0\{\xi - \eta\}\cos(\Theta)\sin(2\Phi) \quad (10)$$

$$p_{010} \equiv -X_0\{\psi - \eta\}\sin(2\Theta) - 2Y_0\,\omega - Z_0\{\xi - \eta\}\sin(\Theta)\sin(2\Phi) \quad (11)$$

$$p_{001} \equiv -X_0\{\xi - \eta\}\cos(\Theta)\sin(2\Phi) - Y_0\{\xi - \eta\}\sin(\Theta)\sin(2\Phi) - 2Z_0\gamma \quad (12)$$

$$p_{000} \equiv -\frac{1}{4} + X_0^2\,\rho + Y_0^2\,\omega + Z_0^2\,\gamma + X_0Y_0\{\psi - \eta\}\sin(2\Theta) + X_0Z_0\{\xi - \eta\}\cos(\Theta)\sin(2\Phi) + Y_0Z_0\{\xi - \eta\}\sin(\Theta)\sin(2\Phi). \quad (13)$$

These equations apply the following definitions:

$$\xi \equiv \{c\,\Delta\tau\}^{-2} \quad (14)$$

$$\eta \equiv \left\{\{c\,\Delta\tau\}^2 - \|\mathbf{x}_r - \mathbf{x}_t\|^2\right\}^{-1} \quad (15)$$

$$\psi \equiv \xi\cos^2(\Phi) + \eta\sin^2(\Phi) \quad (16)$$

$$\gamma \equiv \xi\sin^2(\Phi) + \eta\cos^2(\Phi) \quad (17)$$

$$\rho \equiv \psi\cos^2(\Theta) + \eta\sin^2(\Theta) \quad (18)$$

$$\omega \equiv \psi\sin^2(\Theta) + \eta\cos^2(\Theta). \quad (19)$$

This 3-D ellipsoid is intersected [18] with the ground-plane of $z=0$ to define a 2-D ellipse of possible target locations:

$$\sum_{0\le\alpha+\beta\le 2} p_{\alpha,\beta,0}\; x^\alpha y^\beta = 0. \quad (20)$$

Garren [18] gives a particular procedure for generating alternate target locations for each waveform. One methodology involves the selection of an alternate value of x which lies the overlap of the transmission and reception energy patterns within the ground-plane. The selected fictitious value of x is not required to lie near the true value. Then, use (20) to compute a closed-form value of y:

$$y = \frac{-p_{110}\,x - p_{010} \pm \sqrt{g(x)}}{2\,p_{020}} \quad (21)$$

in terms of the following definition:

$$g(x) \equiv \{p_{110}\,x + p_{010}\}^2 - 4\,p_{020}\{p_{200}\,x^2 + p_{100}\,x + p_{000}\}. \quad (22)$$

The function $g(x)$ must be nonnegative to obtain real-valued solutions for (21). The availability of two solutions of (21) is not an issue since the methodology must only select a location which lies in the overlap region of the transmission and reception beampatterns. Therefore, (21) yields possible alternate locations $\{x, y\}$ of the moving target for each waveform. Garren [18] provides the method for computing the fast-time τ for a given alternate target position $\mathbf{x} \equiv \{x, y\}$ via

$$\tau = \tau_t + \frac{\|\mathbf{x}_t - \mathbf{x}\|}{c}. \quad (23)$$

In summary, this methodology [18] gives an alternate target location and scattering time $\{x_1, y_1, \tau_1\}_{\text{alt}}$ which has the same bistatic range R_1 for the first waveform as that of the true values $\{x_1, y_1, \tau_1\}_{\text{true}}$. This process is used to generate the alternate space-time values $\{x_n, y_n, \tau_n\}_{\text{alt}}$ for each waveform n in the SAR collection interval. Any number of alternate fictitious target trajectories and speed profiles can be generated in this manner.

III. MONOSTATIC COLLECTIONS

Two basic methodologies facilitate the analysis of the SAR target motion ambiguity for cases of monostatic collections. The first is based upon an approximation generated via the bistatic ambiguity equations with the radar transmitter located in close proximity to the receiver. The second is an exact solution found by reducing the equations to simpler form and eliminating unnecessary variables.

A. Approximate Solutions

First, consider the collections wherein the transmitter and receiver are located at exactly identical positions for each waveform of the synthetic aperture. Equations (3) and (4) reveal that the elevation Φ and azimuthal Θ angles are indeterminate, since $\mathbf{w} = \mathbf{0}$ of (2) is not well defined for such cases.

One analysis strategy is to consider a bistatic geometry in which the transmitter and receiver are separated by a small distance, so that Φ and Θ remain well defined. Thus, alternate fictitious target trajectories and speed profiles can be generated corresponding to the true motion of a given target. This method was applied in the monostatic example of [20] wherein the separation between the transmitter and receiver was equal to 2 mm for each waveform of a synthetic aperture. This strategy is expedient given the previous bistatic developments [18] but is insufficient from a theoretical perspective.

B. Exact Solutions

The approximate solutions of Section III-A suggest that exact solutions can be obtained in the limit in which the 3-D ambiguity ellipsoid collapses to a sphere. The specific orientation of the precollapse ellipsoid via the semimajor axis vector $\mathbf{w}$ of (2) determines the specific values of Φ and Θ of (3) and (4). However, an examination of (6)–(13) indicates that the freedom in the ellipsoid orientation and thus that of Φ and Θ seems to yield different values of the $p_{\alpha,\beta,\gamma}$ coefficients.

An alternative approach is to consider the direct case of an exact ambiguity sphere, without the invocation of the collapse from an ellipsoid. For this case, the locations of the transmitter and receiver are exactly identical, i.e., $\mathbf{x}_r = \mathbf{x}_t$. Thus, the semimajor axis vector $\mathbf{w}$ of (2) is equal to the zero vector, so that $\mathbf{w} \equiv \{w_x, w_y, w_z\} = \{0, 0, 0\}$. Therefore, the definitions of Φ and Θ of (3) and (4), respectively, are indeterminate. However, a resolution is provided below.

The assumption of $\mathbf{x}_r = \mathbf{x}_t$ within (14) and (15) implies

$$\xi = \eta = \{c\,\Delta\tau\}^{-2}. \quad (24)$$

Then, (16)–(19) also yield

$$\xi = \eta = \psi = \gamma = \rho = \omega = \{c\,\Delta\tau\}^{-2}. \quad (25)$$

This equation applies for any selection of Φ and Θ.

The use of (25) for monostatic geometries implies that the $p_{\alpha,\beta,\gamma}$ coefficients reduce to the following:

$$p_{200} = p_{020} = p_{002} = \xi \tag{26}$$

$$p_{110} = p_{011} = p_{101} = 0 \tag{27}$$

$$p_{100} = -2X_0\xi, \qquad p_{010} = -2Y_0\,\xi \tag{28}$$

$$p_{001} = -2Z_0\xi \tag{29}$$

$$p_{000} = -\frac{1}{4} + \{X_0^2 + Y_0^2 + Z_0^2\}\xi. \tag{30}$$

It is convenient that the indeterminate angles Φ and Θ of (3) and (4), respectively, vanish entirely from (26)–(30). For the monostatic case, the 3-D ambiguity ellipsoid reduces to a sphere. Thus, the selection of each of the angles Φ and Θ is arbitrary. Furthermore, the choice of these angles is irrelevant, since they vanish from (25)–(30).

Additional simplification is obtained by using (26)–(30) within the 3-D ellipsoid ambiguity (5):

$$\{x^2 + y^2 + z^2 - 2X_0x - 2Y_0y - 2Z_0z + X_0^2 + Y_0^2 + Z_0^2\}\xi - \frac{1}{4} = 0. \tag{31}$$

It is useful to apply (24) in order to replace ξ with $\{c\,\Delta\tau\}^{-2}$. The resulting equation can be factored to yield the intuitive result that the waveform round-trip gives a sphere centered on the instantaneous radar position $\{X_0, Y_0, Z_0\}$:

$$\{x - X_0\}^2 + \{y - Y_0\}^2 + \{z - Z_0\}^2 = \left\{\frac{c\,\Delta\tau}{2}\right\}^2. \tag{32}$$

The intersection of the sphere of (32) with the ground-plane of $z = 0$ yields the ambiguity circle for possible target locations for this particular waveform:

$$\{x - X_0\}^2 + \{y - Y_0\}^2 + Z_0^2 = \left\{\frac{c\,\Delta\tau}{2}\right\}^2. \tag{33}$$

This equation also can be obtained by using (26)–(30) within the 2-D ellipse ambiguity (20).

One possible set of alternate fictitious target trajectories and speed profiles can be generated by selecting some particular set of x values and solving for the required values of y based upon (33), giving

$$y = Y_0 \pm \sqrt{\left\{\frac{c\,\Delta\tau}{2}\right\}^2 - \left\{\{x - X_0\}^2 + Z_0^2\right\}}. \tag{34}$$

This result can be obtained alternatively via (26)–(30) in (21) and (22). Equation (34) is displayed as a single equation but actually applies for each radar range measurement along the synthetic aperture. That is, it applies for an entire set of x values along the SAR collection interval. One possible method for generating a set of x values for an alternate fictitious trajectory is to multiply the true target x values by some scale factor (which can be positive or negative), followed by the addition of a particular offset (which also can be positive or negative).

Garren [18] discusses the result that the value of the fast-time τ corresponding to waveform scattering off of the target is itself ambiguous for general bistatic collection geometries. Specifically, τ is only determined for bistatic collections after an alternate target position $\{x_1, y_1\}_{\text{alt}}$ has been generated via (21). However, for the degenerate case of monostatic collections, the target scattering time τ equals the mid-time of waveform transmission and reception, i.e., $\tau = \{\tau_t + \tau_r\}/2$.

Garren [18], [19] discusses issues pertaining to the inclusion of "range-rate" or Doppler measurements as part of the radar collection. Such information can be obtained by considering two successive range measurements which are collected at times that are separated by a small interval. Thus, the range-rate can be approximated by the difference in the successive range values divided by the time interval between the measurements.

Basically, the computation based upon the difference of two successive ambiguous range measurements yields an ambiguous range-rate result. In addition, this range-rate ambiguity remains in the limit in which the time interval between the range measurements vanishes, so that the ambiguity of the range-rate remains as well for systems which measure Doppler shifts directly. Therefore, the inclusion of range-rate or Doppler information does not remove the fundamental target motion ambiguity discussed herein.

For targets with freedom to move in three dimensions, Garren [19] uses (5)–(19) to generate alternate fictitious trajectories and speed profiles which give the same bistatic range measurements as that of the true target motion. In the degenerate monostatic case, (32) can be applied to solve for a required set of y values corresponding to the selected $\{x, z\}$ coordinates of an alternate fictitious trajectory and speed profile:

$$y = Y_0 \pm \sqrt{\left\{\frac{c\,\Delta\tau}{2}\right\}^2 - \left\{\{x - X_0\}^2 + \{z - Z_0\}^2\right\}}. \tag{35}$$

Again, this single equation enables the computation of the y values for an alternate target trajectory and speed profile for each value of the selected x component values of the target position along the fictitious target trajectory. Application of (35) is straightforward and is left as an exercise to the reader for brevity.

IV. NUMERICAL EXAMPLES

This section presents a particular example in which a monostatic radar travels with constant speed on a straight and level flight path. The radar mainbeam is aimed broadside on the right side of the platform. The radar location at the synthetic aperture mid-point is $\{x, y, z\} = \{0, 6000, 500\}$ in meters. The velocity vector is $\{v_x, v_y, v_z\} = \{200, 0, 0\}$ in m/s. The radar transmits 1001 waveforms at uniform intervals over a 1-s synthetic aperture. The target moves on the ground-plane with average position $\{x, y\} = \{300, 0\}$ m and constant velocity $\{v_x, v_y\} = \{0.5, -5\}$ m/s.

Two alternate sets of target trajectories and speed profiles are generated for the scenario above. The first is obtained by scaling the true target x values by a factor of -1,

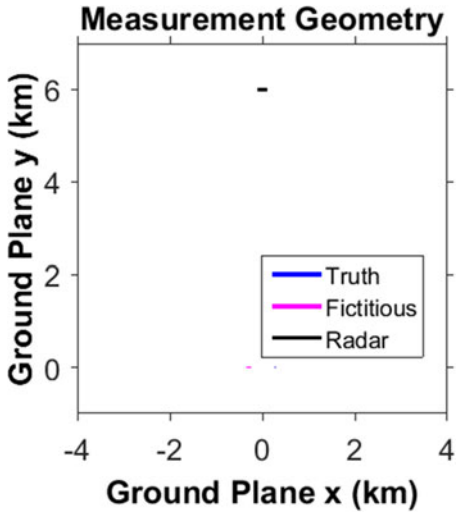

Fig. 1. Collection geometry for the first example.

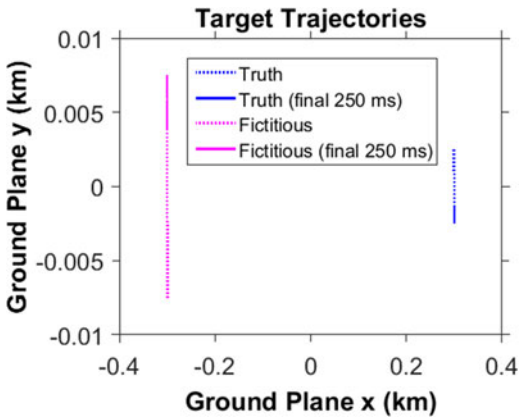

Fig. 2. Zoomed image of the true and first fictitious target trajectories.

followed by a shift of -600 m, for each waveform of the SAR collection. Next, these alternate x values are applied in (34) to compute the corresponding fictitious target y values.

Fig. 1 presents the collection geometry for this example. Here, the trajectories of the true and fictitious targets appear as points in the region of $\{x, y\} = \{0, 0\}$ at this scale. Fig. 2 gives a zoomed image of the local region of the true and fictitious targets, wherein the final 250 ms of the 1000 ms are shown using solid lines, with the remainder given by dotted lines. Thus, the true target moves approximately in the $-y$ direction, and the fictitious target travels approximately in the opposite direction.

Additional insight is obtained by examining a number of the circular wavefronts in the ground plane over the duration of the synthetic aperture. Fig. 3 generates five such wavefronts, corresponding to the following fractions of the full synthetic aperture: $\{0, 0.25, 0.5, 0.75, 1\}$. This figure also shows the locations of the true and fictitious target trajectories of Fig. 2.

Fig. 4 reveals that the speed variation of this first fictitious target is only 0.1 m/s relative to the mean speed of 15 m/s over the 1 s SAR collection. Similarly, Fig. 5 shows that the heading of this alternate target varies by less than

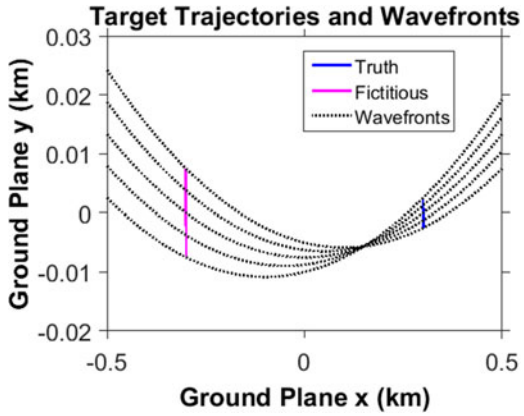

Fig. 3. Zoomed image of the true and first fictitious target trajectories, including five circular wavefronts at the $\{0, 0.25, 0.5, 0.75, 1\}$ fractions of the full synthetic aperture.

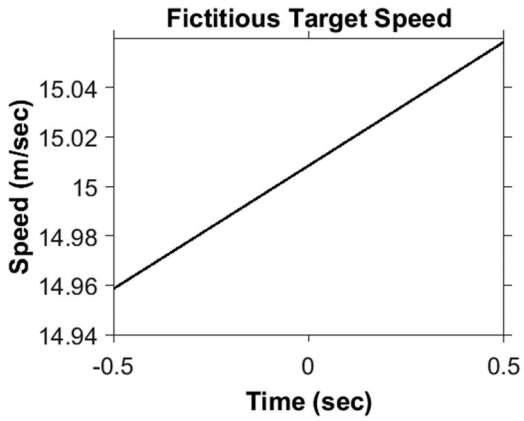

Fig. 4. Speed of the first fictitious target varies by less than 1% over the full SAR collection duration.

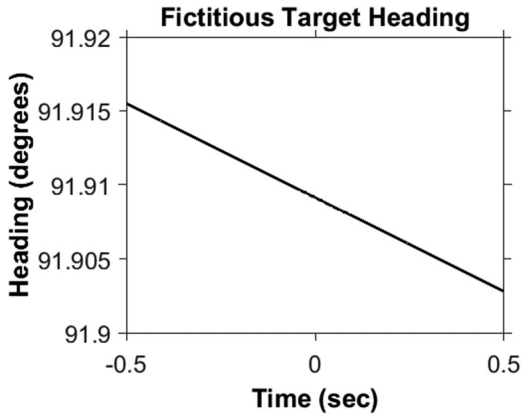

Fig. 5. Heading of the first fictitious target varies by less than 0.1° over the full SAR collection duration.

0.1° over this same time interval. Thus, this alternate target motion corresponds almost to that of constant velocity, and yet it is separated by the relatively large distance of 600 m from the true target location.

Fig. 6 presents a comparison of the range values corresponding to the true target motion and that of the first fictitious target. This figure reveals that the range values are identical to the precision of the machine computations.

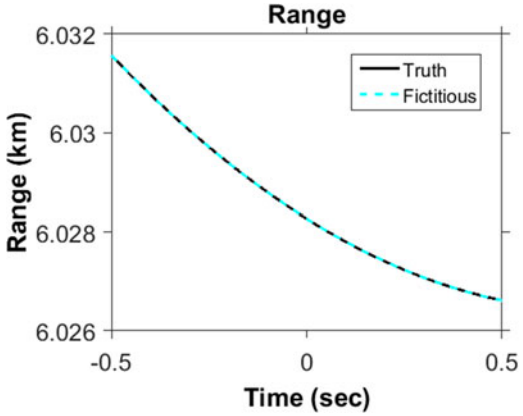

Fig. 6. Range values for the true and fictitious target motions are identical to the precision of the machine computations.

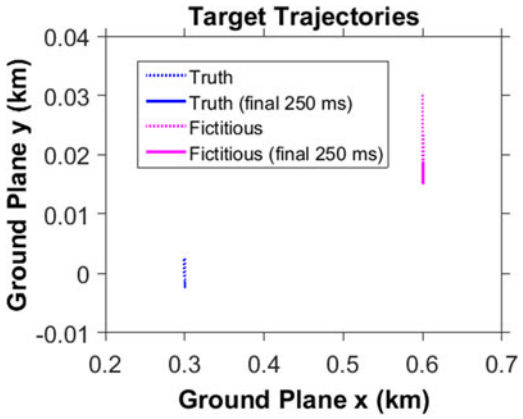

Fig. 7. Zoomed image of the true and second fictitious target trajectories.

The results above are computed using the exact monostatic ambiguity equations generated herein. Garren [20] examines the same monostatic example, albeit using the full bistatic equations of (2)–(23) with a small but nonzero separation of 2 mm between the transmitter and receiver for each waveform. Comparison of the present results with those of Garren [20] yields no perceptible differences. However, the current monostatic equations are significantly simpler to analyze and easier to understand than the general bistatic ambiguity equations.

Next, the present analysis generates a second alternate target trajectory and speed profile. This fictitious target x values for each waveform are obtained by scaling the true target x values by a scale of 1.4, followed by a shift of $+300$ m. The resulting x values are used in (34) to solve for the corresponding fictitious target y values.

Fig. 7 presents the trajectories of the true and second fictitious targets. Both have approximately the same mean heading, but the fictitious target has a significantly higher mean speed. Fig. 8 shows the circular wavefronts at the $\{0, 0.25, 0.5, 0.75, 1\}$ fractions of the full synthetic aperture, together with the trajectories of the true and second fictitious targets. This second fictitious trajectory yields the same range values as in Fig. 6.

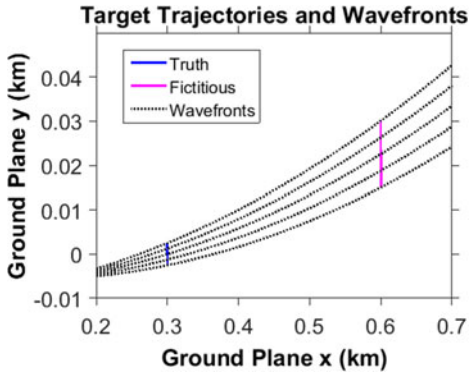

Fig. 8. Zoomed image of the true and the second fictitious target trajectories, including five circular wavefronts evaluated at the $\{0, 1/4, 1/2, 3/4, 1\}$ fractions of the full synthetic aperture.

V. CONCLUSION

Recent studies investigate the ambiguities of bistatic SAR collections by generating fictitious target trajectories and speed profiles which yield the same measurements as those of the true target motion. However, the original bistatic formulation is indeterminate for the degenerate case of exact monostatic geometries. The current analysis resolves these issues and further simplifies the equations for monostatic geometries. Furthermore, the examination of multiple wavefronts over a SAR collection reveals the fundamental nature of these ambiguities.

For the example presented herein, the true target travels with exactly constant velocity and both fictitious targets travel with only minuscule deviations from constant velocity. Yet both fictitious targets are separated by significant physical distances on opposite sides of the true target location. In addition, the headings of the true and first fictitious targets are almost exactly opposite from one another. Thus, there exist significant challenges in determining the values of target motion parameters unless the transmission and reception energy patterns can be made sufficiently narrow. Of course, smaller beam widths have the unfortunate side effect of reducing coverage rates.

In addition, the current monostatic ambiguity analysis has been restricted to case of a single idealized point scattering center. The inclusion of additional scattering centers offers additional constraints on the system of equations based upon the assumption that the distances between the relevant scattering centers do not change throughout the SAR collection process. The impact of such additional constraints on the subject monostatic ambiguities may depend upon the following: 1) the details of the SAR collection, especially, if nonplanar wave-front effects are important, 2) the number and orientation of the additional scattering centers, and 3) nonideal scattering effects, as with scattering from a top-hat reflector. The potential for breaking the subject monostatic ambiguity amid the issues above is beyond the scope of the current Correspondence and is reserved for future work.

Another issue which deserves clarification is that a distinction exists between the estimation of some number of target motion parameters versus the estimation of the complete trajectory and speed profile of a given moving

target. The estimation of certain motion parameter can enable important processing capabilities, as with the refocusing [10] of smeared signatures of moving targets. However, the present generalized analysis reveals that an attempt to estimate the complete target motion trajectory and speed profile yields ambiguities, unless additional constraints are applied [11]–[17].

The mere possibility of a target motion estimation ambiguity can be seen in the equations of Fienup [21] for broadside SAR collections. According to [21, Table II], there are two different "Doppler" contributions to the target phase function which are linear in terms of slow-time: 1) the azimuth or cross-range component of the target position, and 2) the down-range velocity component. Likewise, there are two different "Doppler-rate" contributions to the quadratic target phase variation: 1) the azimuth or cross-range velocity, and 2) the down-range acceleration. This quadratic phase variation is often responsible for a significant portion of the smearing of the SAR signature due to a moving target. The two possible contributions to this quadratic "focus" parameter are effectively a mixture of unknown proportions due to the target cross-range velocity and down-range acceleration. Therefore, a method for estimating this quadratic focus parameter can enable significantly improved target focus, and yet it does not provide any direct information concerning the proportions due to the cross-range velocity component versus that due to the down-range acceleration component.

The existence of multiple possible contributions to these focus parameters is provided for the first and second orders in terms of the slow-time, but [21, Table II] does not provide any information pertaining to higher orders. In effect, it is unclear if these ambiguities exist at higher orders or if they are somehow removed. In addition, examination of higher orders becomes quite cumbersome, and analysis mistakes are more probable.

The current analysis provides a rigorous "proof by contradiction" of the desired ambiguity concepts. That is, we first assume the opposite of which we wish to prove—that is, we *assume* that there does exist a unique target motion estimate for a given set of radar measurements. Next, we generate at least one counter-example in which an alternate fictitious target motion trajectory and speed profile which is significantly different from that of the truth and yet is exactly consistent with the measurement data. Actually, the present analysis generates entire families of such alternate possibilities for the target motion behavior.

The current analysis developed herein is relatively straightforward and perhaps even pedantic to some readers. However, this investigation demonstrates through both basic theory and numerical examples that the use of parametric target motion models can lead to results which are both technically correct and yet simultaneously misleading, since almost imperceptible deviations from such models can yield significantly different conclusions regarding target locations and other motion parameters. Fundamentally, this paper provides a rigorous theoretic foundation of target motion ambiguities for monostatic collection geometries. In addition, this paper should persuade researchers to question any claim of an ability to localize moving targets beyond that which is defined by the real radar aperture beamwidth, unless a realistic set of additional constraints can be invoked. This result applies even if the radar data are measured coherently over a full SAR collection.

ACKNOWLEDGMENT

DoD Distribution Statement A: Unlimited Distribution. The views expressed in this document are those of the author and do not reflect the official policy or position of the Department of Defense or the U.S. Government.

DAVID ALAN GARREN, *Senior Member, IEEE*
Department of Electrical and Computer Engineering, Naval Postgraduate School
Monterey, CA 93943 USA
E-mail: (dagarren@nps.edu)

REFERENCES

[1] J. M. B. Dias and P. A. C. Marques
Multiple moving target detection and trajectory estimation using a single SAR sensor
IEEE Trans. Aerosp. Electron. Syst., vol. 39, no. 2, pp. 604–624, Apr. 2003.

[2] M. Kirscht
Detection and imaging of arbitrarily moving targets with single-channel SAR
IEE Proc.—Radar Sonar Navig., vol. 150, no. 1, pp. 7–11, Feb. 2003.

[3] F. Zhou, R. Wu, and Z. Bao
Approach for single channel SAR ground moving target imaging and motion parameter estimation
IET Radar Sonar Navig., vol. 1, no. 1, pp. 59–66, Feb. 2007.

[4] P. A. C. Marques and J. M. B. Dias
Moving targets processing in SAR spatial domain
IEEE Trans. Aerosp. Electron. Syst., vol. 43, no. 3, pp. 864–874, Jul. 2007.

[5] D. A. Garren
Method and system for developing and using an image reconstruction algorithm for detecting and imaging moving targets
U.S. Patent 7 456 780 B1, Nov. 25, 2008.

[6] J. Yang, C. Liu, and Y. Wang
Imaging and parameter estimation of fast-moving targets with single-antenna SAR
IEEE Geosci. Remote Sens. Lett., vol. 11, no. 2, pp. 529–533, Feb. 2014.

[7] X. Zhang, G. Liao, S. Zhu, C. Zeng, and Y. Shu
Geometry-information-aided efficient radial velocity estimation for moving target imaging and location based on radon transform
IEEE Trans. Geosci. Remote Sens., vol. 53, no. 2, pp. 1105–1117, Feb. 2015.

[8] J. Yang and Y. Zhang
An airborne SAR moving target imaging and motion parameters estimation algorithm with Azimuth-dechirping and the second-order keystone transform applied
IEEE J. Sel. Top. Appl. Earth Observ. Remote Sens., vol. 8, no. 8, pp. 3967–3976, Aug. 2015.

[9] J. Yang, Y. Zhang, and X. Kang
A doppler ambiguity tolerated algorithm for airborne SAR ground moving target imaging and motion parameters estimation
IEEE Geosci. Remote Sens. Lett., vol. 12, no. 12, pp. 2398–2402, Dec. 2015.

[10] C. Noviello, G. Fornaro, and M. Martorella
Focused SAR image formation of moving targets based on doppler parameter estimation
IEEE Trans. Geosci. Remote Sens., vol. 53, no. 6, pp. 3460–3470, Jun. 2015.

[11] M. J. Minardi, L. A. Gorham, and E. G. Zelnio
Ground moving target detection and tracking based on generalized SAR processing and change detection
Proc. SPIE, vol. 5808, pp. 156–165, Jun. 2005.

[12] S. Scarborough, C. Lemanski, H. Nichols, G. Owirka, M. Minardi, and T. Hale
SAR change detection MTI
Proc. SPIE, vol. 6237, pp. 62 370V-1–62 370V-11, May 2006.

[13] M. J. Minardi and E. G. Zelnio
Comparison of SAR based GMTI and standard GMTI in a dense target environment
Proc. SPIE, vol. 6237, pp. 62 370X-1–62 370X-10, May 2006.

[14] M. E. Holston, M. J. Minardi, M. A. Temple, and M. A. Saville
Characterizing geolocation ambiguity responses in synthetic aperture radar: ground moving target indication
Proc. SPIE, vol. 6568, pp. 656 809–1–656 809–11, May 2007.

[15] G. E. Newstadt, E. G. Zelnio, L. Gorham, and A. O. Hero, III
Detection/tracking of moving targets with synthetic aperture radars
Proc. SPIE, vol. 7699, pp. 7699DI-1–7699DI-10, Apr. 2010.

[16] M. Soumekh
Moving target detection if foliage using along track monopulse synthetic aperture radar imaging
IEEE Trans. Image Process., vol. 6, no. 8, pp. 1148–1163, Aug. 1997.

[17] M. I. Pettersson
Detection of moving targets in wideband SAR
IEEE Trans. Aerosp. Electron. Syst., vol. 40, no. 3, pp. 780–796, Jul. 2004.

[18] D. A. Garren
Ambiguities in target motion estimation for general SAR measurements
IET Radar, Sonar Navig., vol. 10, no. 9, pp. 1720–1728, Dec. 2016.

[19] D. A. Garren
Ambiguities in 3D target motion estimation for general radar measurements
IET Radar, Sonar Navig., vol. 11, no. 10, pp. 1523–1529, Oct. 2017.

[20] D. A. Garren
Implications of SAR ambiguities in estimating the motion of slow targets
Proc. SPIE, pp. 102 010E-1–102 010E-13, Apr. 2017.

[21] J. R. Fienup
Detecting moving targets in SAR imagery by focusing
IEEE Trans. Aerosp. Electron. Syst., vol. 37, no. 3, pp. 794–809, Jul. 2001.